

Tracking formulas and strategies for a receiver oriented dual-axis tracking toroidal heliostat

Minghuan Guo^a, Zhifeng Wang^{a,*}, Wenfeng Liang^a, Xiliang Zhang^a, Chuncheng Zang^a,
Zhenwu Lu^b, Xiudong Wei^b

^a Key Laboratory of Solar Thermal Energy and Photovoltaic System of Chinese Academy of Sciences, Institute of Electrical Engineering, Beijing 100190, China

^b Changchun Institute of Optics, Fine Mechanics and Physics, Chinese Academy of Sciences (CAS), Jilin 130033, China

Received 4 September 2009; received in revised form 20 February 2010; accepted 27 February 2010
Available online 24 March 2010

Communicated by Associate Editor L. Vant-Hull

Abstract

A 4 m × 4 m toroidal heliostat with receiver oriented dual-axis tracking, also called spinning-elevation tracking, was developed as an auxiliary heat source for a hydrogen production system. A series of spinning-elevation tracking formulas have been derived for this heliostat. This included basic tracking formulas, a formula for the elevation angle for heliostat with a mirror-pivot offset, and a more general formula for the biased elevation angle. This paper presents the new tracking formulas in detail and analyzes the accuracy of applying a simplifying approximation. The numerical results show these receiver oriented dual-axis tracking formula approximations are accurate to within 2.5×10^{-6} m in image plane. Some practical tracking strategies are discussed briefly. Solar images from the toroidal heliostat at selected times are also presented.

© 2010 Elsevier Ltd. All rights reserved.

Keywords: Heliostat; Toroidal; Tracking

1. Introduction

A 4 m × 4 m toroidal mirror surface heliostat with receiver oriented dual-axis tracking (also called spinning-elevation tracking) was developed in 2007, as shown in Fig. 1. This toroidal heliostat with a secondary concentrator has been used to provide an auxiliary heat source from solar insolation for a hydrogen production system. The main feature of the heliostat was to combine the toroidal mirror surface with spinning-elevation dual-axis tracking. This allows the heliostat optical tangential plane containing the incident solar light at the mirror centre, mirror centre

normal and the reflected light to coincide with the tangential section plane of the heliostat mirror surface in all day.

The compound toroidal mirror surface is composed of 16 identical 1 m × 1 m mirror facets with different curvature radii in the tangential and sagittal directions at the mirror vertex. Each mirror facet has four layers being (a) a supporting layer, (b) a mold formed fibreglass substrate, (c) glue and (d) the 0.4 mm thin glass mirror. Although the toroidal surface is commonly characterised by the tangential circular section and the sagittal circular section, the general definition of the toroidal surface and the optical design method used for this toroidal heliostat prototype are provided elsewhere (Guo et al., 2007).

The basic parameters for the heliostat considered in this work are as follows:

- tangential and sagittal curvature radii at the toroidal mirror vertex, $R_t = 17.079$ m and $R_s = 13.065$ m, respectively,

* Corresponding author. Tel.: +86 10 62520684; fax: +86 10 62587946.
E-mail addresses: zhifeng@vip.sina.com, w_zhifeng@yahoo.com.cn (Z. Wang).

Nomenclature

A, γ_s	solar azimuth angle, $\gamma_s = A - 180^\circ$ is along the south-to-west direction [$^\circ$]	θ	nominal incident angle, equals mirror centre incident angle and elevation angle when no mirror-pivot offset [$^\circ$]
f	on-axis focal length of a spherical or paraboloidal mirror surface [m]	θ', θ^*	elevation tracking angle and mirror centre incident angle of solar beam respectively, $\theta' + \theta^* = 2\theta$ [$^\circ$]
f_t, f_s	tangential focal length and sagittal focal length, respectively [m]	θ_b	elevation biasing angle corresponding to x_b [$^\circ$]
H_z	mirror-pivot offset from the rotation centre to the mirror surface centre [m]	$\theta_b/2 - \varepsilon$	biased elevation angle correction relative to θ , i.e. $\theta' = \theta + \theta_b/2 - \varepsilon$ [$^\circ$]
L	slant distance between the heliostat rotation centre and the target centre [m]	λ	downward tilting angle of the spinning axis from the horizontal [$^\circ$]
R_t, R_s	tangential and sagittal curvature radii at toroidal mirror surface vertex [m]	ρ	counter-clockwise spinning angle [$^\circ$]
x_b	heliostat-centre reflection-point biasing distance from the target centre along the tangential line in the image plane [m]	τ	elevation angle correction for the on-target-centre tracking with a mirror-pivot offset, $\theta' = \theta - \tau$ and $\theta^* = \theta + \tau$ [$^\circ$]
α_s, α	solar altitude angle [$^\circ$]	φ	azimuth angle of the heliostat spinning axis [$^\circ$]
ε	elevation angle correction for a mirror-pivot offset in the case of biased elevation tracking [$^\circ$]		

- heliostat on-axis focal length from mirror surface centre to its focal point, $f = L_0 = 7.4689$ m,
- slant distance between the heliostat rotation centre and the target centre, $L = 7.486$ m,
- mirror-pivot offset from the rotation centre to the mirror surface centre, $H_z = 0.460$ m,
- downward tilting angle of the spinning axis from the horizontal, $\lambda = -19.6955^\circ$, local latitude $\Phi = 34.260^\circ\text{N}$,
- azimuth angle of the heliostat spinning axis from north to east $\varphi = 180^\circ$ (the spinning axis pointing to South), and longitude is 108.980°E .

The SPA astronomical solar position algorithm (Reda and Andreas, 2004), with a maximum error less than 0.0003° , was adopted to give the sun position for the

toroidal heliostat. A series of tracking formulas based on vector geometry have been derived. These include (a) basic spinning-elevation, (b) spinning-elevation with mirror-pivot offset and (c) biased elevation angle with mirror-pivot offset, and are discussed in more detail in later sections.

Some practical tracking strategies were applied to this heliostat, such as

- the use of a high accuracy theodolite to survey the pointing direction of the heliostat spinning axis,
- using a mini flat mirror attached on the centre of the heliostat frame to observe the reflected sun trace on the target plane to assess tracking error, and

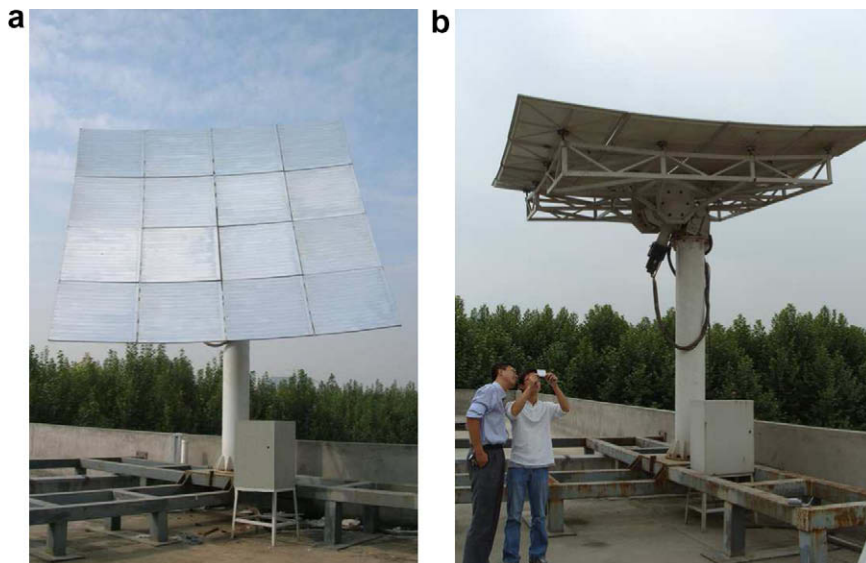


Fig. 1. Photos of the toroidal heliostat on a rooftop at Xi'an Jiaotong University in China: (a) front view showing mirror and (b) side view showing support structure.

(c) the on-Sun alignment of the mirror facets on the heliostat frame after tracking parameter adjustment.

To improve and maintain the tracking accuracy, on one cloudless day of each season, the focused solar image on the receiver aperture was manually moved to the aperture centre on the exact hour. From this, the precise hourly angles on that day were obtained for both tracking axes, allowing correction of tracking angles via linear interpolation over a full (solar) day.

This paper discusses the derivation of the tracking formulas and briefly introduces the practical tracking strategies.

2. Overview of dual-axis tracking modes

Generally a dual-axis tracking mode has one tracking axis fixed to the foundation and the other perpendicular to the fixed one, as a slave axis. A number of dual-axis tracking modes are mentioned in the literature (Lipps and Vant-Hull, 1978), such as alt-azimuth, radial-pitch-roll, azimuth-pitch-roll, polar and the receiver oriented. These variations of sun tracking are due to the heliostat being a rigid body with three degrees of rotational freedom while the two orthogonal axes serve for orientating the heliostat centre normal to the expected direction. The third degree of rotational freedom is redundant and reserved for the heliostat structure. Since different tracking modes lead to different heliostat orientations and most heliostat geometries are not circular symmetrical, the reflected solar images on the image plane are different. Reversing the fixed-and-slave roles of the two axes results in two different tracking modes, such as the pair of the alt-azimuth and the pitch-roll (horizontal axis is fixed).

The alt-azimuth dual-axis tracking mode is widely adopted for the sun-trackers, solar dishes and heliostats. However, pitch-roll tracking has the potential to permit a more compact array of heliostats than alt-azimuth tracking (Schramek and Mills, 2004). For dual-axis polar tracking, the fixed axis is parallel to the polar axis of the earth, and it rotates at a constant clockwise speed. The receiver-oriented tracking is discussed later in some detail.

Igel and Hughes (1979), have analysed the astigmatism of the focusing reflectors with a spherical surface of radius $R = 2*f$, and the off-axis imaging was given as $f_t = f*\cos \theta$ and $f_s = f/\cos \theta$. Here f is the on-axis focal length, θ is the incident angle, f_t and f_s are the tangential focal length and sagittal focal length, respectively. The toroidal surface, defined by the orthogonal radii, $R_t = 2f/\cos \theta$ and $R_s = 2f*\cos \theta$ was used to approximate the equivalent auto-adaptive paraboloidal surface of the central receiver optical system.

The work of Rabl (1985) has also qualified the off-axis aberrations of spherical reflectors. Zaiabel et al. (1995) considered the concept of a target aligned heliostat with a combination of receiver oriented dual-axis tracking and toroidal surface. The fixed axis of such a heliostat points

to the target centre, the slave axis is fixed with respect to the heliostat frame and always along the sagittal direction of the mirror frame. This enables a toroidal surface with different sagittal and tangential radii at the vertex to be exploited to reduce the astigmatism of the spherical mirror for the non-normal solar incidence.

3. Basic spinning-elevation tracking formulas

Given a toroidal heliostat without mirror-pivot offset, the spinning-elevation angles can be derived based solely on the geometry of the solar vector and the spinning axis pointing vector since the tracking angles are only determined by the position relationship of the sun, the target centre and the heliostat centre.

The spinning-elevation tracking geometry is shown in Fig. 2. In Fig. 2(a) the point **O** stands for the heliostat pivot, with vectors **OT**, **ON**, **OS** being the spinning axis pointing to the target centre, mirror normal and the solar vector, respectively; **OP₀** perpendicular to **OT** is the zero spinning position, and the tangential plane Π of the heliostat containing **OP₀**, **ON** and **OT** is perpendicular to ground plane. In Fig. 2(b), the heliostat is tracking such that vector **OP₀** moves to **OP** position around **OT**, while the vectors **OS**, **OP**, **OT** and the mirror normal **ON'** are all within the tangential plane Π' . θ is the incident angle, the elevation angle $\angle \text{TON}' = \theta$, ρ is the counter-clockwise spinning angle, and $\angle \text{P}_0\text{OP} = -\rho$.

The left-hand coordinate system [**O**; North-East-Height] results in the following equations:

$$\mathbf{OS} = (\cos \alpha \cos A, \cos \alpha \sin A, \sin \alpha) \tag{1}$$

$$\mathbf{OT} = (\cos \lambda \cos \phi, \cos \lambda \sin \phi, -\sin \lambda) \tag{2}$$

Here, λ is the downward tilting angle of the spinning axis from the horizontal, α and A are the solar altitude angle and the solar azimuth angle in north eastward direction, respectively.

$$\cos(2\theta) = \mathbf{OT} \cdot \mathbf{OS} \tag{3}$$

$$\sin(2\theta)\mathbf{OP} = \mathbf{OS} - \cos(2\theta)\mathbf{OT} \tag{4}$$

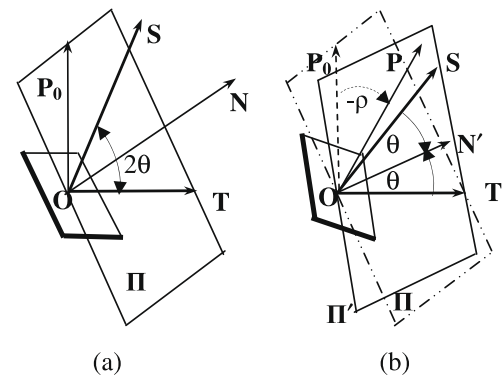


Fig. 2. Schematic of the spinning-elevation tracking geometry: (a) shows the initial spinning position and (b) shows the expected counter-clockwise spinning angle ρ from **OP₀** to **OP** and the elevation angle θ from **OT** to **ON'**.

$$\mathbf{OP}_0 = (\sin \lambda \cos \phi, \sin \lambda \sin \phi, \cos \lambda) \quad (5)$$

$$-\sin \rho \mathbf{OT} = \mathbf{OP}_0 \times \mathbf{OP} \quad (6)$$

$$\cos \rho = \mathbf{OP}_0 \times \mathbf{OP} \quad (7)$$

It follows that

$$\begin{aligned} \cos \rho &= \mathbf{OP}_0 \cdot (\mathbf{OS} - \cos(2\theta)\mathbf{OT}) / \sin(2\theta) \\ &= \mathbf{OP}_0 \cdot \mathbf{OS} / \sin(2\theta) \\ &= [\sin \lambda \cos \alpha \cos(A - \varphi) + \cos \lambda \sin \alpha] / \sin(2\theta) \end{aligned} \quad (8)$$

$$\begin{aligned} \sin \rho &= \sin \rho \mathbf{OT} \cdot \mathbf{OT} \\ &= -[\mathbf{OP}_0 \times (\mathbf{OS} - \cos(2\theta)\mathbf{OT}) / \sin(2\theta)] \cdot \mathbf{OT} \\ &= -(\mathbf{OP}_0 \times \mathbf{OS} \cdot \mathbf{OT}) / \sin(2\theta) \\ &= \sin(A - \varphi) \cos \alpha / \sin(2\theta) \end{aligned} \quad (9)$$

Following equations (3), (8), and (9), the tracking angle expressions in vector form are derived as

$$\theta = 0.5 \arccos(\mathbf{OT} \cdot \mathbf{OS}) \quad (10)$$

$$\rho = -\arg[\mathbf{OP}_0 \cdot \mathbf{OS} + \mathbf{i}^*(\mathbf{OP}_0 \times \mathbf{OS} \cdot \mathbf{OT})] \quad (11)$$

From Eqs. (3), (8), and (9), the tracking expressions in terms of the angular parameters are rewritten as

$$\begin{aligned} \theta &= 0.5 \arccos(-\sin \lambda \sin \alpha + \cos \lambda \sin \varphi \cos \alpha \sin A \\ &\quad + \cos \lambda \cos \varphi \cos \alpha \cos A) \end{aligned} \quad (12)$$

$$\begin{aligned} \rho &= \text{sign}[\sin(A - \varphi)] \arccos\{[\sin \lambda \cos \alpha \cos(A - \varphi) \\ &\quad + \cos \lambda \sin \alpha] / \sin(2\theta)\}. \end{aligned} \quad (13)$$

The above tracking formulas, in Eq. (10)–(13), were derived from the tracking geometry using the vector geometry. These equations are basic tracking angle formulas for the spinning-elevation tracking heliostat without mirror-pivot offset.

The sun position in the sky is commonly estimated by Eqs. (14) and (15) in solar engineering applications because of their simplicity.

$$\alpha = \arcsin(\sin \delta \sin \Phi + \cos \delta \cos \delta \cos \omega \cos \Phi) \quad (14)$$

$$A = 180^\circ + \text{sign}(\sin \omega) \arccos\left(\frac{\sin \alpha \sin \Phi - \sin \delta}{\cos \alpha \cos \Phi}\right) \quad (15)$$

These two equations can be used to check the validity of the basic tracking angle formulas. Fig. 3(a) shows the solar position angles in terms of the solar hour on 21st December based on Eqs. (14) and (15), but what is plotted is really $\alpha_s = \alpha$ and $\gamma_s = A - 180^\circ$, and the solar azimuth in the plot is along the south-to-west direction. Fig. 3(b) shows the corresponding spinning-elevation tracking angles based on Eqs. (12) and (13). The spinning angle illustrated in Fig. 3(b) is along the right-hand rotation direction, and when the heliostat is tracking the sun, the heliostat top orients east in the morning, upward at noon, and west in the afternoon.

A possible case of “ $\theta = 0^\circ$ ” for Eqs. (11) and (13), when the sun vector coincides with the fixed axis, would mean the spinning angle effectively flips through 180° when the sun passes through the target centre. This discontinuity may cause the driving mechanism to stagnate. A smooth spinning motion can be achieved by either (a) setting $\theta = -\theta$

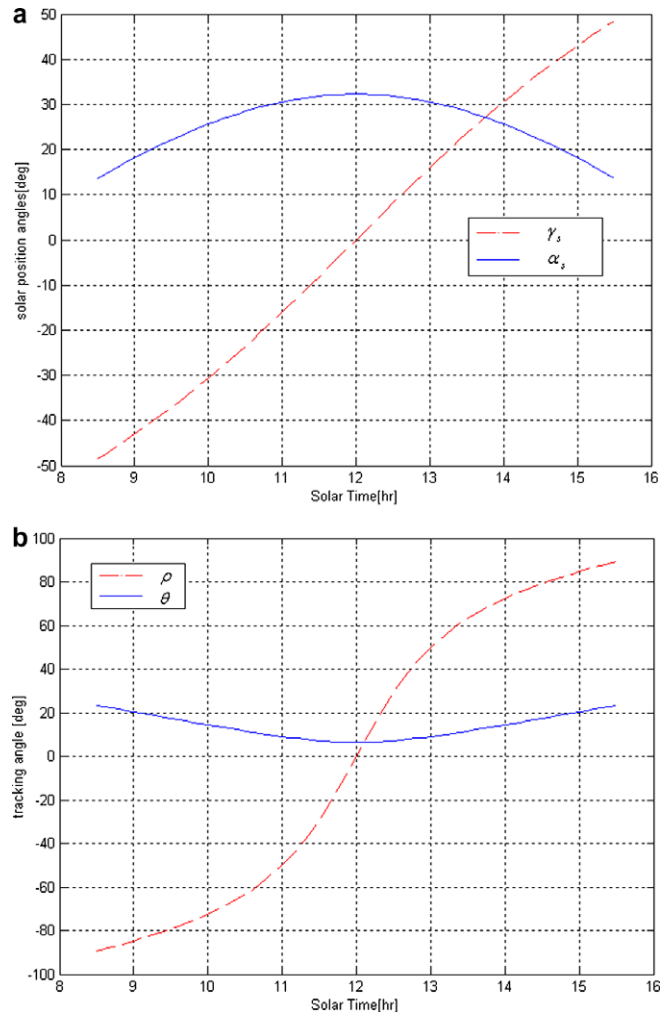


Fig. 3. Solar position angles and tracking angles based on solar time for 21st December: (a) Solar azimuth angle, $\alpha_s = \alpha$, and solar altitude angle, $\gamma_s = A - 180^\circ$ in a south-to-west direction and (b) spinning-elevation tracking angles.

and $\rho = \rho - 180^\circ$, or (b) simply rapidly move the spinning angle to the next expected position.

4. Spinning-elevation tracking angles for a mirror-pivot offset heliostat

The offset of the mirror centre from the heliostat pivot has no effect on the spinning angle. The basic spinning angle (13) is the exact tracking angle, and hence we only require consideration of the elevation angle correction for a mirror-pivot offset heliostat.

The heliostat-centre reflection-point is defined as the intercept between the reflected light from the centre of the heliostat mirror and the image plane (target plane) which is perpendicular to the spinning axis. If the heliostat-centre reflection-point is not in the centre of the target, a correction to the elevation angle is required. A mechanism for describing and determining the elevation angle correction, τ , follows.

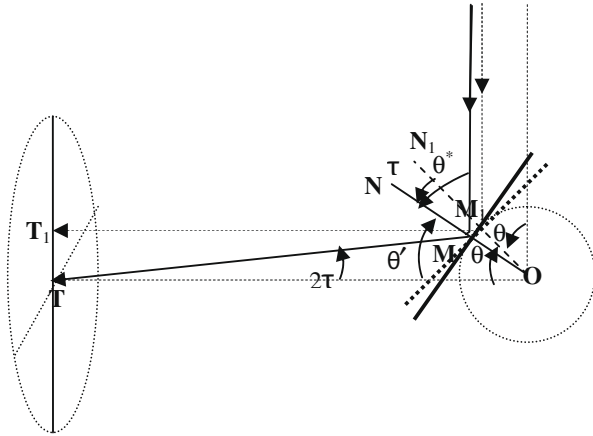


Fig. 4. Schematic of the diagram for the exact elevation angle correction τ in the tangential profile plane with respect to the nominal incident angle θ .

The geometry to develop the exact elevation angle correction, τ , for a given nominal incident angle θ is shown in Fig. 4. In this figure, OT is the fixed spinning axis pointing to the target centre, angle τ is used for adjusting the reflected central light from M_1T_1 to MT , $\theta' = \theta - \tau$ and $\theta^* = \theta + \tau$ are the elevation tracking angle and the incident angle of the central light, respectively. The slant distance from the heliostat pivot to the target centre, is noted as $OT = L$, and the radius of circle O equals mirror-pivot offset H_z .

According to the reflection geometry in Fig. 4, in $\triangle OMT$, the following equation holds:

$$L \sin(2\tau) = H_z \sin \theta^* = H_z \sin(\theta + \tau) \quad (16)$$

If substituting $b = L/H_z$, yields

$$2b \sin \tau \cos \tau = \sin \theta \cos \tau + \cos \theta \sin \tau \quad (17)$$

By substituting $t = \cos \tau$, $\sin \tau$ can be eliminated by trigonometric substitution, yielding

$$4b^2 t^4 - 4b \cos \theta t^3 + (1 - 4b^2)t^2 + 4b \cos \theta t - \cos^2 \theta = 0 \quad (18)$$

Eq. (18) is a 4th order polynomial in terms of variable t , so a numerical solution can be easily obtained, and the exact elevation angle correction is expressed as

$$\tau = \arccos\{\text{root}([4b^2, -4b \cos \theta, (1 - 4b^2), 4b \cos \theta, -\cos^2 \theta])\} \quad (19)$$

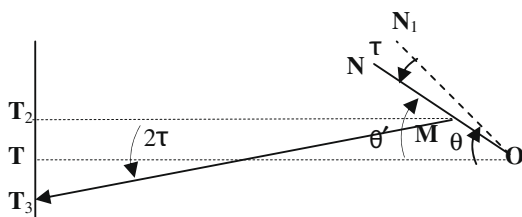


Fig. 5. Schematic of the diagram for the residual error analysis of the elevation angle $\theta' = \theta - \tau$ in the tangential profile plane.

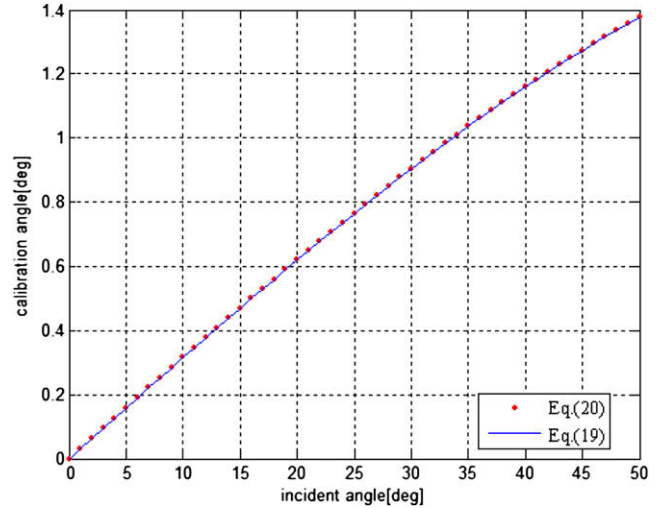


Fig. 6. Comparison of the exact Eq. (19) and approximate Eq. (20) elevation angle corrections.

Since τ has a small positive value (see Fig.6) due to the small ratio of H_z/L , an approximation is possible by substituting $\cos \tau = 1$ into Eq. (17),

$$\tau = \arcsin\left(\frac{H_z \sin \theta}{2L - H_z \cos \theta}\right) \quad (20)$$

In this approximation the three terms in Eq. (17) are positive, τ has a small positive value, and both sides increase with the approximation of $\cos \tau = 1$, so the balance of Eq. (17) remains and provides a high degree of precision.

In Fig. 5, θ is the nominal incident angle, OT is the fixed spinning axis, τ is the elevation angle correction, ON is the current mirror normal at the central point M , MT_3 is the reflection central light impinging on the image plane.

By comparing Fig. 5 to 4, we can easily estimate the residual error of the elevation tracking with respect to any τ , and express it as

$$\begin{aligned} x_e &= \underline{T_2T} - \underline{T_2T_3} \\ &= H_z \sin(\theta - \tau) - [L - H_z \cos(\theta - \tau)] \tan(2\tau) \end{aligned} \quad (21)$$

The residual error determination from Eq. (21) is used to compare the precision of the two elevation correction formulas Eqs. (19) and (20). Fig. 6 shows the correction for the elevation angle versus the nominal incident angle for Eq. (19) “exact” elevation angle correction and Eq. (20) approximate elevation angle correction. Over the nominal incident angle range $[0^\circ, 50^\circ]$, the maximum residual error for the approximate elevation angle correction, Eq. (20), is less than 2.5×10^{-6} m. This means the approximation in Eq. (20) can be used instead of the exact elevation angle correction in Eq. (19).

5. Biased elevation angle for a mirror-pivot offset heliostat

Since the toroidal surface is symmetrical, the image centroid is on the tangential line of the image plane intercepted

by the tangential plane of the heliostat. In principle, the heliostat-centre reflection-point differs from the image centroid. In practice, the tracking error is measured in terms of the image centroid, so the bias between the image centre and the heliostat-centre reflection-point should be considered. Given a bias point on the tangential line in the image plane relative to the target centre, if we know the bias between the heliostat-centre reflection-point and the image centroid, we can adjust the image centroid to the target centre using a biased elevation angle correction with respect to the nominal incident angle.

In Fig. 7, the biasing angle θ_b corresponds to the biasing target centre, T_b , on the tangential line in the image plane; angle ε is for the mirror normal adjustment from ON_1 to ON so as to compensate the mirror-pivot offset. θ , θ' and θ^* are the nominal incident angle, biased elevation tracking angle and the incident angle of the central light of solar beam on the mirror centre, respectively. It is apparent that

$$2\theta = \theta' + \theta^* = 2\theta_0 + \theta_b. \tag{22}$$

$$\theta_0 = \theta - \theta_b/2. \tag{23}$$

$$\theta' = (\theta_b + \theta_0 - \varepsilon) = (\theta + \theta_b/2 - \varepsilon) \tag{24}$$

$$\theta^* = (\theta_0 + \varepsilon) = (\theta - \theta_b/2 + \varepsilon) \tag{25}$$

In $\triangle OMT_b$, $\angle OT_bM = 2\varepsilon$, $\angle OMT_b = 180^\circ - \theta^* = 180^\circ - (\theta_0 + \varepsilon)$, $a = OT_b = L/\cos \theta_b$, the mirror-pivot offset $OM = H_z$, and the following equation holds:

$$H_z \sin \theta^* = a \sin(2\varepsilon) = a \sin(2\theta^* - 2\theta_0) \tag{26}$$

If $\beta = -2\theta_0$ and $s = a/H_z$, then

$$\sin \theta^*/s = 2 \sin \theta^* \cos \theta^* \cos \beta + (1 - 2 \sin^2 \theta^*) \sin \beta \tag{27}$$

Thus

$$4s^2 t^4 + 4bt^3 + (1 - 4s^2)t^2 - 2bt + b^2 = 0 \tag{28}$$

where $b = s^* \sin \beta$ and $t = \sin \theta^*$. The solution of Eq. (28) is expressed as

$$\sin \theta^* = \text{root}([4s^2, 4b, (1 - 4s^2), -2b, b^2]) \tag{29}$$

The same approximation strategy as that used to derive Eq. (20) from Eq. (17) for the elevation angle correction can be used to approximate the biased elevation angle θ' from Eq. (29).

From Eq. (25) and (26),

$$a \sin(2\varepsilon) = H_z \sin \theta^* = H_z \sin(\theta_0 + \varepsilon) \tag{30}$$

Since $\sin 2\varepsilon = 2 \sin \varepsilon \cos \varepsilon$, and $\sin(\theta_0 + \varepsilon) = \sin \theta_0 \cos \varepsilon + \sin \varepsilon \cos \theta_0$

$$2a \sin \varepsilon \cos \varepsilon = H_z (\sin \theta_0 \cos \varepsilon + \cos \theta_0 \sin \varepsilon) \tag{31}$$

Assuming ε is small, $\cos \varepsilon = 1$ can be substituted into Eq. (31), to give the approximation

$$\sin \varepsilon = \left(\frac{H_z \sin \theta_0}{2a - H_z \cos \theta_0} \right) \tag{32}$$

and

$$\varepsilon = \arcsin \left(\frac{H_z \sin(\theta - \theta_b/2)}{2L/\cos \theta_b - H_z \cos(\theta - \theta_b/2)} \right) \tag{33}$$

Comparing Eq. (33) with Eq. (20), it can be seen that Eq. (20) is the special case of Eq. (33) when the biasing angle $\theta_b = 0^\circ$.

In Fig. 8, OT is the fixed spinning axis, θ_b is biasing angle, ε is correction angle for the mirror-pivot offset H_z , ON is the current mirror normal at the central point M , MT_{b1} is the reflection central light impinging on the tangential line in the image plane. θ^* is the incident angle on the mirror centre, and the immediate angle $\theta_b - 2\varepsilon$ is used

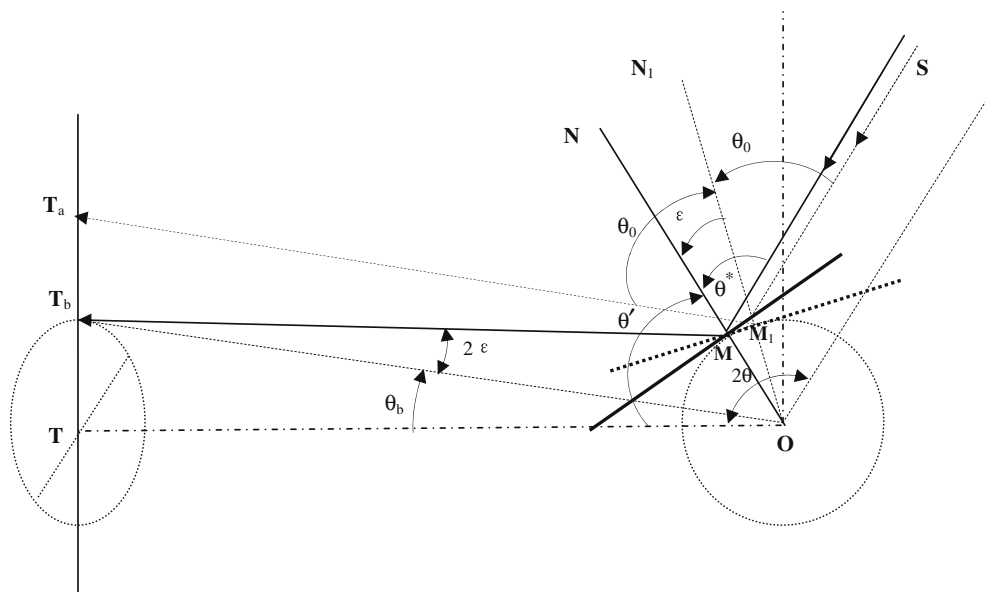


Fig. 7. Schematic diagram for the biased elevation angle θ' in the tangential profile plane corresponding to the nominal incident angle θ and the biasing angle θ_b . In this figure, OT is the fixed spinning axis, the immediate angle ε is used for adjusting the reflected central light from M_1T_a to MT_b , θ^* is the solar incident angle at the mirror centre. And the identical equation is $2\theta = \theta' + \theta^* = 2\theta_0 + \theta_b$.

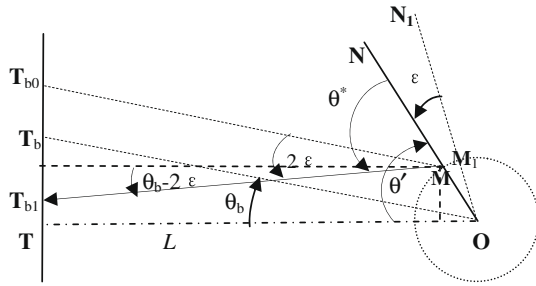


Fig. 8. Schematic diagram for the residual error analysis of the biased elevation angle $\theta' = \theta - \theta_b/2 - \epsilon$ in the tangential profile plane.

to estimate the tracking residual error along the tangential line in image plane.

According to Fig. 8, $x_b = TT_b = L \tan \theta_b$, $x_{bI} = TT_{bI} = H_z \sin \theta' + (L - H_z \cos \theta') \tan(\theta_b - 2\epsilon)$, so the residual error of the biased elevation tracking is

$$x_e = x_{bI} - x_b = L[\tan(\theta_b - 2\epsilon) - \tan \theta_b] + H_z[\sin \theta' - \cos \theta' \tan(\theta_b - 2\epsilon)] \quad (34)$$

Eq. (34) can be used to check the precision of the biased elevation angle $\theta' = \theta + \theta_b/2 - \epsilon$ from Eq. (33), by comparing it to the exact elevation tracking angle $\theta' = 2\theta - \theta^*$ from Eq. (29), given a heliostat-centre reflection-point biasing $x_b = 0.1$ m and mirror-pivot offset of 0.460 m. Based on the residual error from Eq. (34). The tracking error increases approximately from zero at normal incidence to a negligible two microns at 45° . This means that the elevation tracking angle $\theta' = \theta + \theta_b/2 - \epsilon$ from the approximation in Eq. (33) can be used instead of the exact biased elevation angle $\theta' = 2\theta - \theta^*$ from Eq. (29). Based on Eq. (33), the lines of θ , θ' and θ^* over the nominal incident angle range of $[0^\circ, 50^\circ]$ are shown in Fig. 9, the symmetry along the diagonal line of θ , as can be explained by Eqs. (24) and (25), and the interception point of these three lines is positioned by the correction angle $\theta_b/2 - \epsilon$ relative to θ .

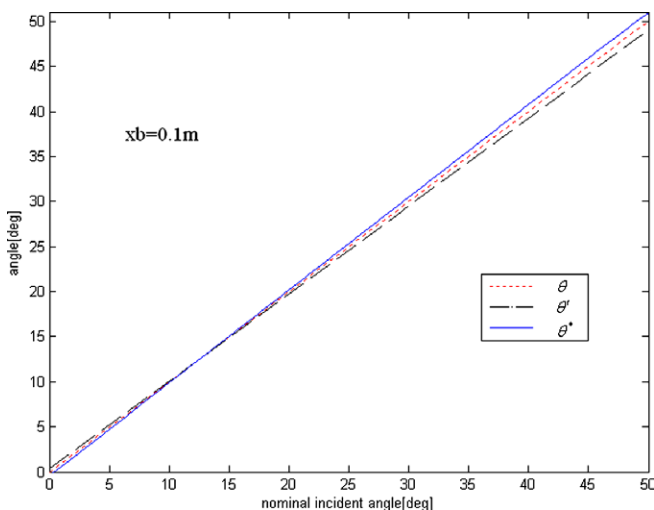


Fig. 9. Relationship between the biased elevation angle, mirror centre incident angle and the nominal incident angle, given a heliostat-centre reflection-point biasing $x_b = 0.1$ m and mirror-pivot offset of 0.460 m.

In the example illustrated in Fig.9, the biasing angle θ_b is constant over the whole incident angle range, but it can be adaptive according to the aiming requirements of the heliostat-centre reflection-point on the image plane. Therefore, it is in effect a function of nominal incident angle. This exact biased elevation formula is useful for further analysis of the tracking error sources and to further improving tracking accuracy. This provides an extension version of the elevation tracking correction formula presented in Section 4 considering the mirror-pivot offset.

6. Some simple strategies for practical heliostat tracking

6.1. Measurement of on-spot heliostat geometry by the high precision trimble survey

A high precision theodolite (Trimble S6S DR STA/1"1 mm + 1 ppm) was used to survey the receiver-heliostat geometry, and the pointing direction (azimuth angle and altitude angle) of the fixed spinning axis with a 360° active prism firmly mounted on the heliostat frame and step-rotating around the axis. In principle, the surveyed points are on a circular arc, and three and more points can determine the normal of the scanning plane parallel to the axis. Given position of the elevation axis, the tilt angle from horizontal can be found by the same method. Thus, the zero position of the elevation axis is determined. The three-dimension coordinates of the heliostat pivot can be solved via step-rotation surveying the two tracking axes

6.2. Check the tracking accuracy and adjust the tracking parameters

One tracking test performed on the heliostat utilized a small flat mirror on the heliostat frame centre with all heliostat mirror facets either being shaded or removed. The reflected spot on the temporary target was observed when the heliostat was smoothly tracking the sun. A small flat mirror was glued onto the centre of the clear glass board attached on the heliostat frame centre to form a reflected spot on the testing target. From the spot trace, some tracking parameters were adjusted. The effectiveness of this method is dependent upon whether the mini mirror facet is orthogonal to the spinning axis of the heliostat. So the procedure of aligning the clear glass board normal to the spinning axis is very important. At least, the mini mirror should be parallel to the elevation axis, since the mirror normal variance in the tangential plane is easier to calibrate. In our work, the heliostat was first rotated to " $\rho = 0^\circ$ " around the spinning axis, then rotated to the flat state around the elevation axis as shown for the heliostat orientation in Fig. 1(b).

6.3. Tracking strategy to fix the image centroid to the target centre

Section 5 proposes the exact biased elevation angle formula allowing biased elevation tracking to be applied to

adjust the image centroid to the target centre. If the difference between the image centroid and the heliostat-centre reflection-point is known as the function of the nominal incident angle, then the control strategy needs to aim the biased point when the image centroid coincides with the target centre.

In practice, however, the heliostat performance is constrained by a combination of error sources whose magnitude is variable and time dependent. Both the elevation angle and the spinning angle precision are limited by variable error sources, so the biased elevation tracking angle is adopted both for the nominal incident angle and time.

For the toroidal heliostat, data was recorded at hourly intervals by moving the image centroid to the target centre, and recording the tracking angles (elevation angle and spinning angle). These recorded tracking angles are notated as θ'_i and ρ_i , $i = 1, \dots, I$, so the differences between recorded tracking

$$d\theta_i = \theta'_i - \theta'(t_i) \quad (35)$$

$$d\rho_i = \rho_i - \rho(t_i) \quad (36)$$

Then $d\theta_i$ and $d\rho_i$ were linearly interpolated to the entire (solar) day. The real tracking angles at the time interval $[t_i, t_{i+1}]$ of any day in this season are thus expressed as

$$\theta_{real}(t, n) = \theta'_n(t) + \frac{(t_{i+1} - t)d\theta_i + (t - t_i)d\theta_{i+1}}{t_{i+1} - t_i} \quad (37)$$

$$\rho_{real}(t, n) = \rho_n(t) + \frac{(t_{i+1} - t)d\rho_i + (t - t_i)d\rho_{i+1}}{t_{i+1} - t_i} \quad (38)$$

where n is the day index, θ'_n and ρ_n are the n th day biased elevation angle and the spinning angle in terms of time t ,

respectively. This process and determination was repeated seasonally.

7. Concentrated solar images on a temporary target

A series of solar images on a white-painted temporary steel target representing a receiver aperture were taken on 14th March 2009 using a normal digital camera. Although we are still not satisfied with the image size and shape, the image photos give a good illustration of the receiver-oriented tracking. This used the tracking strategy in Section 6.3. The six images at Beijing times of 11:10, 12:46, 13:19, 15:01 and 16:41, are shown in Fig. 10. Fig. 10(b) shows the whole heliostat under the solar image test. The target size is $1 \text{ m} \times 1 \text{ m}$, and the square marked on the target was $0.6 \text{ m} \times 0.6 \text{ m}$. From Fig. 10, it can be seen that the solar image is changing with time in shape and size, and rotating around the target centre in a clockwise direction. The solar image at 13:19 is near solar noon, and Beijing time 11:10 and 15:01 are nearly symmetric about solar noon, so the solar image in Fig. 10(a) seems symmetric to the solar image in Fig. 10(d). The solar image at 16:41 is quite different to the solar image 15:01, since the mirror centre incident angle of the solar beam increases by about 9° , from 22.9° to 32.0° (Table 1), giving a significant change in the cosine of the incidence angle.

The corresponding angles at the five specific times for the toroidal heliostat are listed in Table 1. These include the solar altitude angle and azimuth angle (in south-to-west direction) computed using SPA astronomical solar position algorithm, the nominal incident angle θ based on Eq. (12), spinning angle ρ based on Eq. (13), elevation angle $\theta' = \theta - \tau$ and incident angle of the central light of solar

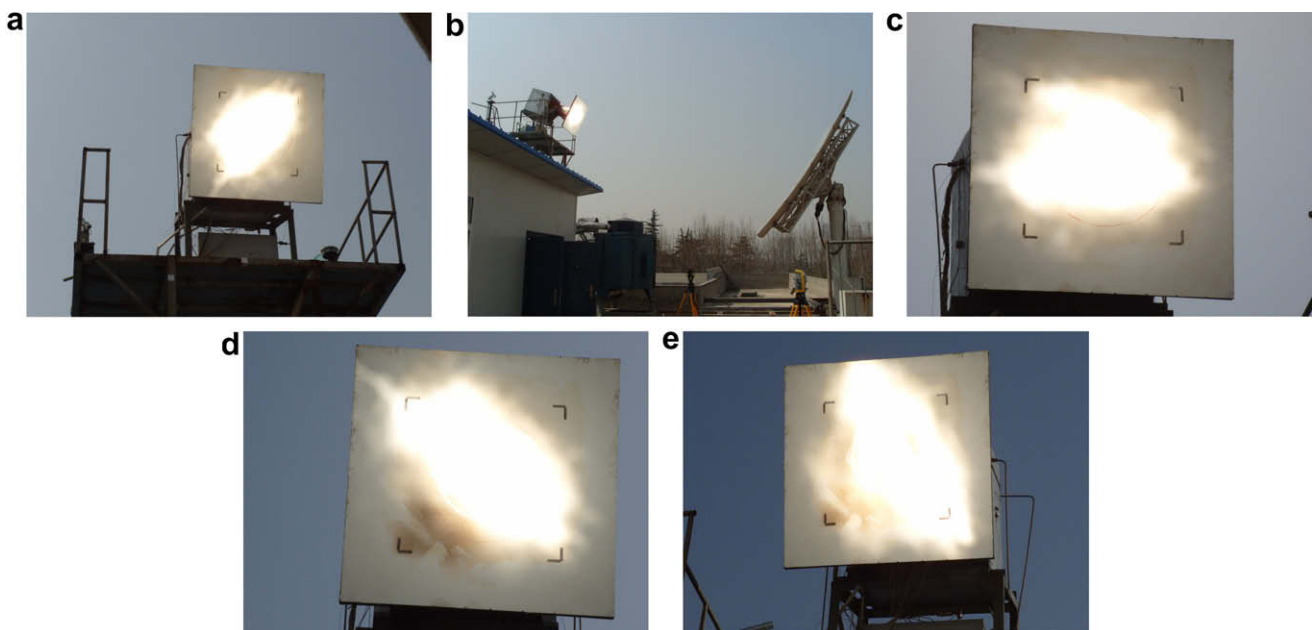


Fig. 10. Concentrated solar images of the toroidal heliostat taken at Beijing time: (a) 11:10, (b) 12:46, (c) 13:19, (d) 15:01 and (e) 16:41 on 14th March 2009.

Table 1
Computed solar angles and the heliostat tracking angles at given times.

Beijing Time	11:10	12:46	13:19	15:01	16:41
March 14, 2009					
Solar altitude [°]	45.8	53.0	52.6	42.5	25.2
Solar azimuth [°]	−38.7	−3.1	10.5	45.7	67.6
Nominal incident angle [°]	20.5	16.7	16.9	22.3	31.0
Spinning angle [°]	−41.6	−3.4	11.5	48.8	71.2
Elevation angle [°]	19.9	16.2	16.4	21.6	30.1
Mirror centre incident angle, θ^* [°]	21.1	17.2	17.5	22.9	32.0
Cosine(θ^*)	0.93	0.96	0.95	0.92	0.85

beam on the mirror centre, $\theta^* = \theta + \tau$, derived from Eq. (20). Since the real elevation angle and the spinning angle shown on the controlling computer of the heliostat were not recorded, they are not presented in Table 1.

Future work will be directed at improving the mirror surface accuracy, mirror facet alignment accuracy and redesign of mirror surface shape to match the current fixed heliostat-and-receiver geometry on the narrow building roof. In addition, we need to also model and analyse the concentration of the receiver oriented toroidal surface heliostat considering the multiple error sources.

8. Conclusion

A prototype of a receiver oriented toroidal surface heliostat with spinning-elevation tracking has been set up and tested in Xi'an with nearly two year's operation.

A series of spinning-elevation tracking formulas for the prototype have been derived. This series included basic tracking formulas, formulas for the elevation angle for heliostat with a mirror-pivot offset, and more general formulas for the biased elevation angle. The basic tracking formulas were derived using vector algebra based solely on sun-heliostat-target geometry, and are easy to combine with any solar vector model. The basic tracking formulas expressed in angular parameters are convenient for tracking engineering, while the expressions in vector form clearly reflect the receiver-oriented tracking geometry. For a heliostat with a mirror-pivot offset, both the tracking formula of the on-target-centre elevation angle and the formula of the biased elevation angle are good approximations of the

solution of the elevation angle equations. Analysis of the tracking residual error shows the accuracy is sufficient to compensate for the effect of the mirror-pivot offset. In addition to these tracking formulas, some helpful strategies have been applied in the tracking practice of the toroidal heliostat.

The exact tracking formulas provide a good foundation for further analysis of the heliostat tracking error, since a real heliostat always suffers from many error sources. In addition, the exact tracking angles are useful for analysis and assessment of concentrated solar images on a receiver aperture.

Acknowledgements

We gratefully acknowledge the financial support of National Basic Research Program of China (No. 2003CB214500). We want to thank staff of the State Key Laboratory of Multiphase Flow in Power Engineering in Xi'an Jiaotong University for their warm assistance in the installation and test of the heliostat. We also like to say thanks to Steve McEvoy, Jim Hinkley, Sarah Miller and Wes Stein at CSIRO Australia for revising the paper. Last but not least, we greatly appreciate Lorin Vant-Hull's helpful comments on the paper draft before submitting.

References

- Guo, M.H., Wang, Z.F., Lu, Z.W., 2007. The optical designing method and the concentrating performance analysis for a toroidal heliostat with spinning-elevation sun tracking. In: Proceedings of Ises Solar World Congress 2007: Solar Energy and Human Settlement, vols. I–V, pp. 1878–1882.
- Reda, I., Andreas, A., 2004. Solar position algorithm for solar radiation applications. *Solar Energy* 76, 577–589.
- Lipps, F.W., Vant-Hull, L.L., 1978. A cellwise method for solar central receivers systems. *Solar Energy* 20, 505–516.
- Schramek, Philipp, Mills, David R., 2004. Heliostats for maximum ground coverage. *Energy* 29, 701–713.
- Igel, E.A., Hughes, R.L., 1979. Optical analysis of solar facility heliostat. *Solar Energy* 22, 283–295.
- Rabl, A., 1985. *Active Solar Collectors and their Applications*. Oxford University Press, USA.
- Zaibel, R., Dagan, E., Karni, J., Ries, H., 1995. An astigmatic corrected target-aligned heliostat for high concentration. *Sol. Energy Mater. Sol. Cells* 37, 191–202.